ORIGINAL ARTICLE

Amyloid oligomerization of the Parkinson's disease related protein α-synuclein impacts on its curvature-membrane sensitivity

José Ignacio Gallea*, Ernesto E. Ambroggio*, Aldo Alejandro Vilcaes*, Nicholas G. James†, David M. Jameson† and María Soledad Celej* [ID]

*Centro de Investigaciones en Química Biológica de Córdoba, CIQUIBIC, CONICET and Departamento de Química Biológica Ranwel Caputto, Facultad de Ciencias Químicas, Universidad Nacional de Córdoba, Haya de la Torre y Medina Allende, Ciudad Universitaria, X5000HUA Córdoba, Argentina

†Department of Cell and Molecular Biology, John A. Burns School of Medicine, University of Hawaii at Manoa, Honolulu, Hawaii

Abstract

The amyloid aggregation of the presynaptic protein α-synuclein (AS) is pathognomonic of Parkinson's disease and other neurodegenerative disorders. Physiologically, AS contributes to synaptic homeostasis by participating in vesicle maintenance, trafficking, and release. Its avidity for highly curved acidic membranes has been related to the distinct chemistry of the N-terminal amphipathic helix adopted upon binding to appropriated lipid interfaces. Pathologically, AS populate a myriad of toxic aggregates ranging from soluble oligomers to insoluble amyloid fibrils. Different gain-of-toxic function mechanisms are linked to prefibrillar oligomers which are considered as the most neurotoxic species. Here, we investigated if amyloid oligomerization could hamper AS function as a membrane curvature sensor. We used fluorescence correlation spectroscopy to quantitatively evaluate the interaction of oligomeric species, produced using a popular method based on lyophilization and rehydration, to lipid vesicles of different curvatures and compositions. We found that AS oligomerization has a profound impact on protein-lipid interaction, altering binding affinity and/or curvature sensitivity depending on membrane composition. Our work provides novel insights into how the formation of prefibrillar intermediate species could contribute to neurodegeneration due to a loss-of-function mechanism.

Keywords: FCS, lipid-protein interaction, neurodegeneration, protein aggregation, synucleinopathies, toxic oligomers.

J. Neurochem. (2018) **147**, 541–556.

α-synuclein (AS) is a small, natively unfolded presynaptic protein highly expressed in dopaminergic neurons (Iwai *et al.* 1995). Its pathological deposition in Lewy bodies is a hallmark of a number of devastating neurodegenerative disorders, such as Parkinson's disease (PD), PD with dementia and multiple system atrophy, collectively referred to as synucleinopathies that affect over 5 million people worldwide (Lashuel *et al.* 2013). Structurally, AS is characterized by a Lys-rich N-terminus (Met^1-Lys^{60}) which is crucial in modulating membrane interaction, a hydrophobic aggregation-prone central region (Glu^{61}-Val^{95}) and an acidic C-terminal domain (Lys^{96}-Ala^{140}) that modulates fibrillogenesis (Fig. 1a).
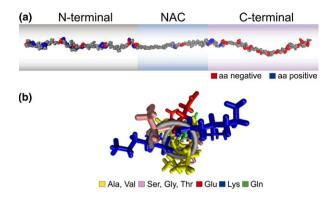
Although its precise function remains elusive, substantial evidences point to a possible role of AS in regulating synaptic homeostasis (Auluck *et al.* 2010; Lashuel *et al.*

2013). Indeed, alterations in the physiological level of AS are associated with deficiencies in dopamine release and deregulations in the population and recycling of synaptic

ORIGINAL ARTICLE

Fig. 1 Structural features of AS. (a) Schematic representation of AS functional domains. (b) Amphipathic properties of the N-terminal region of AS (PDB 1XQ8, only the segment encompassing residues Ser^9-Ala^{30} are shown for better visualization).

vesicles (SVs) (Murphy *et al.* 2000; Cabin *et al.* 2002; Larsen *et al.* 2006; Nemani *et al.* 2010). Overexpression of AS diminishes neurotransmitter release by inhibiting SVs priming (Larsen *et al.* 2006) or reclustering after endocytosis (Nemani *et al.* 2010). On the other hand, reduced levels of AS decrease the number of distal SVs (Murphy *et al.* 2000; Cabin *et al.* 2002) and impairs replenishment of docked vesicles at synapses from the distal reserve pool (Cabin *et al.* 2002). In addition, AS can also assist in synaptic functions by interacting with synaptic proteins. AS cooperates with cysteine-string protein-α (CSP-α) and SNAREs proteins in preventing neurodegeneration (Chandra *et al.* 2005), and promotes SNARE-complex assembly by simultaneously binding to phospholipids via its N-terminus and to the v-SNARE synaptobrevin-2 via its C-terminus (Burré *et al.* 2010) inducing SVs clustering (Diao *et al.* 2013).

In line with the observations pointing toward the important role of AS in synaptic vesicle maintenance, trafficking and release, *in vitro* studies show that AS has a greater affinity for highly curved anionic vesicles (Davidson *et al.* 1998; Middleton and Rhoades 2010), similar in size to SVs. Upon binding to membranes, the N-terminal and central regions of the protein adopt a helical structure whereas the C-terminus remains unbound and disordered (Davidson *et al.* 1998; Eliezer *et al.* 2001; Bodner *et al.* 2009; Fusco *et al.* 2014). When bound to vesicles of ~ 30 nm, the extended and curved α-helix spans over 90 aa in length (Jao *et al.* 2008). More recently, Fusco *et al.* (2014) showed that the segment of the N-terminal domain encompassing residues Lys^6-Gly^{25} forms a well-defined amphipathic α-helix acting as a membrane anchor whereas the central segment (Val^{26}-Lys^{97}) is more dynamic and adopts an α-helix structure when transiently bound to lipid interfaces, modulating AS affinity for membranes depending on their lipid composition. The dual sensitivity of AS to both membrane charge and curvature seems to be related to the distinct chemical characteristic of

its extended amphipathic helix (Antonny 2011; Pranke *et al.* 2011). AS has a poorly developed hydrophobic phase made of small residues, such as Val, Ala, and Thr, and a well-developed charged polar phase with an almost balanced distribution of Lys residues at the interface and Glu residues forming a crest (Antonny 2011; Pranke *et al.* 2011) (Fig. 1b). Whereas the basic residues would confer a greater affinity for anionic lipids, the unbalanced chemistry of the amphipathic helix would provide a special sensitivity for curved and less packed membranes (Antonny 2011; Pranke *et al.* 2011).

Similar to other amyloid diseases, prefibrillar soluble oligomers are considered to be the most neurotoxic species (Lashuel *et al.* 2013; Chiti and Dobson 2017). Different pathways of pathobiology have been attributed to these species, such as the impairment of biomembranes, the establishment of aberrant intermolecular interactions, the interference with the cellular protein quality and clearance systems and the cell-to-cell spreading of the pathology, among others (Ingelsson 2016; Cremades *et al.* 2017). In addition to these gain-of-toxic function mechanisms, oligomers could also drive an abnormal vesicle cycling at the synapses by altering lipid interactions. In this study, we employed fluorescence correlation spectroscopy (FCS) to quantitatively assess the interaction between monomers (mAS) or oligomers (oAS) of AS with vesicles of varying lipid compositions and sizes. We found that AS oligomerization has a profound impact on the protein-lipid interaction properties, showing a distinct binding affinity and curvature sensitivity as compared to mAS.

Materials and methods

Materials

1-palmitoyl-2-oleoyl-sn-glycero-3-phosphoserine (POPS, Cat# 840034P), 1-palmitoyl-2-oleoyl-sn-glycero-3-phosphocholine (POPC, Cat# 850457P), 1-palmitoyl-2-oleoyl-sn-glycero-3-phosphoglycerol (POPG, Cat# 84045P), 1-palmitoyl-2-oleoyl-sn-glycero-3-phos-phoethanolamine (POPE, Cat# 850757P) and cholesterol (Chol, Cat# 700000P) were obtained from Avanti Polar Lipids (RRID: SCR_016391). Alexa Fluor 488 C$_5$ maleimide (A488) dye (Cat# A10254) was from Invitrogen (RRID:SCR_013318). All other reagents were of analytical grade.

Protein expression, purification and labeling

The sequence encoding for human wild-type AS cloned into the pT7-7 expression vector was a kind gift of Dr T. Jovin (Max Planck Institute for Biophysical Chemistry, Göttingen, Germany). Because the wild-type protein does not contain any Cys residue in its sequence necessary for specific labeling with thiol-reactive fluo-rophores, Ala at position 140 was replaced by Cys (mAS-A140C). In addition, the codon 136 within the coding sequence of both wild-type and mAS-A140C was changed from TAC to TAT to prevent Cys misincorporation upon bacterial expression (Masuda *et al.* 2006). Modifications in the open reading frames ware made by

GenScript Corporation (RRID:SCR_002891), and they were confirmed by DNA sequencing.

AS was expressed in *E.coli* BL21(DE3) cells (Cat# CMC0014, Sigma-Aldrich, RRID:SCR_008988) and purified as previously described (Gallea and Celej 2014). Briefly, bacteria were transformed and grown at 37°C under constant shaking at 250 rpm in LB medium supplemented with ampicillin (100 µg/mL) to an OD_{600}=0.6. Protein expression was induced with 0.5 mM IPTG (Cat# I2481C5, Genbiotech, Buenos Aires, Argentina) at 37°C for 4 h, and the cells were harvested by centrifugation at 4000 *g* for 15 min (Sorvall RC 6 Plus Superspeed Centrifuge, Thermo Scientific, RRID:SCR_008452)). The pellet was resuspended in 10 mM Tris-HCl pH 8.0, 1 mM EDTA, 1 mM phenylmethylsulfonyl fluoride (PMSF) and lysed by three freeze-thaw cycles and sonication. The cell lysate was boiled for 30 min and centrifuged at 13 000 *g*. Streptomycin sulfate (10 mg/mL) was added to the supernatant, and the mixture was stirred for 15 min at 4°C and centrifugated as before. Upon addition of $(NH_4)_2SO_3$ (360 mg/mL) to the supernatant, the solution was stirred and centrifuged as before. The pellet was resuspended in 25 mM Tris-HCl pH 7.7, loaded onto an anion exchange column (POROS HQ, Applied Biosystems, RRID:SCR_005039) on an Äkta purifier (GE Healthcare RRID: SCR_000004), and eluted with a 0–600 mM NaCl salt gradient. The single Cys variant was expressed and purified as the wild-type protein, with the addition of 5 mM dithiothreitol (DTT, Cat# DTT5, Genbiotech, Buenos Aires, Argentina) in the elution buffer to avoid disulfide bridge formation. Proteins were dialyzed against HEPES buffer (150 mM NaCl, 10 mM HEPES (Cat# H3375-25G, Sigma-Aldrich, RRID:SCR_008988), pH 7.5), with the addition of 5 mM DTT in the case of mAS-A140C, and stored at −20°C until further use. The protein purity was assessed by sodium dodecyl sulfate–polyacrylamide gel electrophoresis and the protein concentrations were determined by absorbance (ϵ^{275}=5600 M^{-1} cm^{-1}).

The mAS-A140C variant was fluorescently labeled with A488 dye following manufacturer's protocol (Invitrogen, RRID:SCR_013318). After removing any precipitate by centrifugation, samples were concentrated in Amicon Ultra-4 10 kDa cut-off filters (Cat# UFC801024, Millipore RRID:SCR_008983) and kept overnight at 4°C in the presence of 0.1 M guanidinium chloride as an additional step to remove any dye non-specifically bound to the protein, and then dialyzed against HEPES buffer. Protein concentration of the labeled monomers (mAS-A488) was determined by the Lowry assay using mAS (quantified by absorbance) as standard for the calibration curve. The labeling efficiency, typically > 95%, was calculated using ϵ^{495} = 72 000 M^{-1} cm^{-1} (Haugland and Spence 2005).

Oligomer formation

We used a simple method based on freeze-drying of concentrated samples (Volles *et al.* 2001; van Rooijen *et al.* 2009a; Celej *et al.* 2012; Gallea and Celej 2014; Gallea *et al.* 2016; Fusco *et al.* 2017) to produce stable β-sheet rich AS oligomers. Briefly, 300 µM stock solutions were prepared by mixing mAS and mAS-A488 to give an initial label density of 14%. After lyophilization, samples were redissolved in HEPES buffer and centrifuged (20 000 *g*, 30 min, 4°C) to remove big particles. Sub-stoichiometrically labeled oligomers (oAS-A488) were separated from the monomer by filtration at 4°C using Amicon Ultra-0.5 100kDa cut-off filters (Cat# UFC510096, Millipore RRID:SCR_008983). The procedure

was repeated until the fluorescence intensity of the probe detected in the flow-through was negligible as compared with the intensity measured in the retentate. With this protocol we typically obtained ~100–150 µM oAS-A488 stock solutions, expressed in monomeric units as measured by the Lowry assay. The removal of the monomeric protein was confirmed by native gradient PAGE, the absence of amyloid fibrils was verified by Thioflavin T fluorescence, the morphology of the oligomers was assessed by transmission electron microscopy and their secondary structure features were characterized by attenuated total reflectance-Fourier transform-infrared spectroscopy (Figure S1).

Native gradient PAGE

Native polyacrylamide gels were cast with a linear gradient from 4 to 15% and silver-stained. HMW native marker (Cat# 17044501, GE Healthcare RRID:SCR_000004) was loaded as the molecular mass marker. Electrophoresis was performed under non-denaturing conditions at a constant 60 V and 4°C.

Thioflavin T (Thio T) fluorescence assay

Corrected emission spectra were acquired with a Cary Eclipse spectrofluorimeter (Agilent Technologies, RRID:SCR_013575), using excitation at 446 nm, spectral bandwidths of 10 nm and a 1 cm path cuvette. Experiments were performed at 25°C using final concentrations of 0.25 µM protein and 5 µM dye. A488 fluorescence contribution was subtracted in all cases.

Transmission electron microscopy (TEM)

Samples (5 µL) were adsorbed onto Formvar-coated carbon grids (200 mesh), washed with Milli-Q water, and stained with 1% (w/v) uranyl acetate. The samples were imaged in a JEM-1200 Ex (Jeol) transmission electron microscope equipped with a GATAN camera, model 785.

Attenuated total reflectance Fourier transform infrared spectroscopy (ATR–FTIR)

IR spectra were acquired on a Nexus IR spectrophotometer (Nicolet) equipped with a single reflection diamond reflectance accessory (Golden Gate, Specac, Fort Washington, PA, USA) continuously purged with dried air. The samples (~2 µL) were spread on a diamond crystal surface and flushed with nitrogen. A total of 256 accumulations were recorded at 25°C using a resolution of 2 cm^{-1}. After subtraction of water vapor and side chain contributions, the spectra were baseline corrected and area normalized between 1600 and 1700 cm^{-1}. The spectra were Fourier self-deconvoluted with a resolution enhancement factor K = 1.8 for a better visualization of the overlapping components arising from de distinct structural elements. Spectra were processed and analyzed using Kinetic software developed at the Structure and Function of Membrane Biology Laboratory, Université Libre de Bruxelles, Brussels, Belgium.

Dot blot

Samples were spotted on to a nitrocellulose membrane and dried at 25°C for 30 min. After blocking for 1 h with 10% (w/v) non-fat dried skimmed milk powder in 0.01% TBST (Tris-buffered saline/Tween20; 10 mM Tris-HCl, pH 8, 150 mM NaCl and 0.01% Tween 20) and washing with 0.01% TBST, the membrane was incubated

with a rabbit anti-synaptophysin antibody (anti-SYP, Cat# A0010, DakoCytomation, Glostrup, Denmark) for 3 h at 25°C (1 : 1000) in 0.01% TBST. After washing three times with 0.01% TBST, blots were probed with IRDye 800CW anti-rabbit IgG (1 : 15000, Cat# 926-32211, Li-Cor Biosciences, Lincoln, NE, USA), washed as before and scanned using an Odyssey infrared scanner (Li-Cor Biosciences).

Vesicle preparation

Vesicles of various compositions were prepared by mixing the lipids from stock solutions in chloroform/methanol (2:1 v/v), dried under nitrogen flow, and placed in vacuum overnight. The resulting lipid film was rehydrated in HEPES buffer for 1 h. For the preparation of large unilamellar vesicles (LUVs), aqueous lipid solutions were extruded 25 times through polycarbonate membranes (100 nm pore diameter) at 25°C. For the preparation of small unilamellar vesicles (SUVs), rehydrated lipids were freeze-thawed five times by dipping into liquid nitrogen and thawing above the lipid phase transition temperature. The preparations were then sonicated three times during 5 min on a Cole Parmer Ultrasonic Homogenizer at 50% duty circle. SUVs were centrifuged at 14 000 g for 30 min to remove big particles. SVs were isolated from mouse brains (see below). All vesicles were assayed for inorganic phosphate to determine the total lipid concentration (Fiske 1925). For the mixture containing cholesterol, the total lipid concentration was calculated by adding a 25% to the phospholipid determination. The sizes of the vesicles were characterized by dynamic light scattering (DLS) using a Nicomp 380 sub-micrometer particle sizer (Particle Sizing Systems, Port Richey, FL, USA) in the volume weighing Gaussian distribution mode. The diameters were between 16 and 35 nm for SUVs, 74–84 nm for LUVs and ~35 nm for SVs.

Purification of synaptic vesicles

SVs were purified according to the protocol described by Ahmed *et al.* (2013) as described in detail in the Supporting information. Briefly, the brains of two young (6-8 weeks) male wild-type C57BL/6J mice (stock 000664, The Jackson Laboratory, RRID: IMSR_JAX:000664) were obtained and homogenized in 4 mM HEPES buffer pH 7.4, 320 mM sucrose at 4°C supplemented with protease inhibitor. Large cell fragments, nuclei and synaptosomes were separated by centrifugation. The supernatant was stored at 4°C until further use (S1). Synaptosomes were exposed to a hypotonic solution to release SVs and centrifuged to remove large membrane particles. The recovered supernatant (S2) was combined with supernatant S1 and centrifuged. 5 mL of the supernatant was placed on a 5 mL cushion of a 0.7 M sucrose solution (in duplicate) and ultracentrifuged for 1 h at 4°C to separate the SVs from macro-molecular complexes. Then, it was divided into aliquots of 500 μL and those enriched in SVs were collected. A last ultracentrifugation was performed to recover the SVs in the precipitate. For the dissociation of peripheral proteins, the SVs suspension was incubated in a solution of Na$_2$CO$_3$ pH12 at 4°C for 30 min and successive washed with 100 mM Tris-HCl buffer pH 7.6, 100 mM KCl using Amicon Ultra-0.5 100kDa cut-off filters (Cat# UFC510096, Millipore RRID:SCR_008983). The presence of SVs was confirmed by dot blot with an anti-synaptophysin antibody, an integral membrane protein of these vesicles. With this procedure a SVs preparation of ~35 nm (> 95%) determined by DLS was achieved.

FCS measurements

The measurements were performed on an Olympus FV1200 scanning confocal microscope equipped with a 60 × 1.3 silicone immersion objective and a solid-state 473 nm laser (Olympus Corporation, Shinjuku, Tokyo, Japan). Measurements were made on cover glasses that were first passivated with a solution of 1% albumin to prevent AS adsorption to the glasses surfaces. The laser focus was positioned in the solution ~15 μm above the top surface of the cover glass. Fluorescence data were acquired for 91 s, and the resulting image (256 × 32766 pixels) was analyzed using the Globals-simFCS 4 software (developed by E. Gratton, Laboratory of Dynamic Fluorescence, University of California, Irvine, CA, USA).

The structure factor s, the ratio of the radial to axial dimensions of the focal volume, was determined with fixed fluorescent nanoparticles (Cat# T14792, TetraSpeck fluorescent microspheres size kit, Invitrogen, RRID:SCR_013318) giving a value of 0.25. This value agreed well with the determination of s as a free parameter for solutions of fluorescein sodium salt dye ($D = 430$ μm^2 s^{-1}) and was fixed for all subsequent fittings.

Partition studies were performed in HEPES buffer at a constant protein concentration (100 nM mAS-A488 and 1000 nM oAS-A488) and varying lipid concentrations. The same population of LUVs or SUVs was employed to assess the interaction with monomers or oligomers. The samples at different lipid/protein ratio were allowed to equilibrate for 30 min at 23°C prior to data acquisition.

Thirty-three autocorrelation curves were averaged and analyzed with the autocorrelation function $G_{(\tau)}$ which accounts for two distinct species diffusing in a three-dimensional Gaussian volume (Thompson 1991):

$$G(\tau) = \frac{1}{N}\left[\left(1 - F_{AS}^b\right)\frac{1}{1 + \frac{\tau}{\tau_{AS}}}\left(\frac{1}{1 + \frac{s^2\tau}{\tau_{AS}}}\right)^{\frac{1}{2}}\right.$$
$$\left. + F_{AS}^b\frac{1}{1 + \frac{\tau}{\tau_{AS}^b}}\left(\frac{1}{1 + \frac{s^2\tau}{\tau_{AS}^b}}\right)^{\frac{1}{2}}\right] \tag{1}$$

where N is the number of fluorescent particles, $1 - F_{AS}^b$ is the fraction of AS free in solution, F_{AS}^b the fraction of AS bound to the vesicle, τ_{AS} and τ_{AS}^b the diffusion times of free and vesicle-bound AS, respectively. The subscript AS refers to mAS-A488 or oAS-A488. The values for τ_{AS} and τ_{AS}^b were determined independently from the autocorrelation curves of protein alone or in the presence of an excess of lipid, which were fitted with a function for a single diffusing species:

$$G(\tau) = \frac{1}{N}\left[\frac{1}{1 + \frac{\tau}{\tau_{AS}}}\left(\frac{1}{1 + \frac{s^2\tau}{\tau_{AS}}}\right)^{\frac{1}{2}}\right] \tag{2}$$

and then were fixed in the partition experiments. This procedure implies that the diffusing species are similar in their brightness. Such a requirement is fulfilled if all of them contain a single fluorophore and if the interaction does not change either its absorption or quantum yield.

Titration curves were constructed by plotting the F_{AS}^b values extracted from eqn 2 as a function of the accessible lipid concentration ($[L]_{acc}$). These curves were analyzed considering a partition equilibrium between two immiscible fluid phases, the aqueous and lipid phase. Thus, for a non-cooperative interaction, the molar fraction of the vesicle-bound protein through both electrostatic and hydrophobic interactions is (White *et al.* 1998):

$$F_{AS}^b = \frac{K_p[L]_{ac}}{[\text{H}_2\text{O}] + K_p[L]_{ac}} \tag{3}$$

where K_p is the partition coefficient and $[\text{H}_2O] = 55,3\ M$ is the molar concentration of water. Thus, the free energy of partitioning is defined by $\Delta G_p^o = -RTlnK_p$.

Due to its wide use in the literature, titration curves were alternatively fitted with eqn 4 considering a dynamic binding equilibrium:

$$F_{AS}^b = \frac{[L]_{acc}}{K_d^{app} + [L]_{acc}} \tag{4}$$

to obtain the apparent dissociation constant K_d^{app}.

To calculate $[L]_{acc}$, we considered the fraction of lipids in the outer monolayer (x_{ac}) which corresponds to the ratio between the surface area of the outer leaflet and the total area, according to:

$$x_{acc} = \frac{(4\pi r_{out}^2)}{(4\pi(r_{in}^2 + r_{out}^2))} = \frac{r_{out}^2}{((r_{out} - d)^2 + r_{out}^2)} \tag{5}$$

where r_{in} y r_{out} are the radii of the inner and outer membrane leaflets respectively, and the difference between them is the thickness of the bilayer, d. Finally, at a given total lipid concentration $[L]_{tot}$, the concentration of accessible lipid is: $[L]_{acc} = x_{acc}[L]_{tot}$. r_{out} for the different vesicles were experimentally determined by DLS and $[L]_{tot}$ by the Fiske-Subbarow technique (Fiske 1925) as described before. d values for vesicles of pure lipids were: POPG 4.45 nm, POPS 4.45 nm and POPC 4.05 nm (Dickey and Faller 2008). In the cases of lipid mixtures, d was approximated as the thickness given by the most abundant lipid.

Statistical analysis

The study did not involve pre-registration, randomization, or blinding. All animal procedures were reviewed and approved by the Institutional Review Board and Ethical Committee (IAUCC Res. N° 832/2015 renewed in 2017) of Facultad de Ciencias Químicas, Universidad Nacional de Córdoba. Partition experiment were performed at least in duplicate and analyzed independently. FCS curves with more than two standard deviations from the averaged autocorrelation curve were identified as outliers, manually curated and removed from the analysis. Diffusion times were obtained through fitting the FCS data considering a 3D Gaussian distribution. The FCS and titration data were analyzed using a Marquardt-Levenberg non-linear least squares fitting routing incorporated in Microcal Origin software (RRID:SCR_002815). The goodness of the fittings was judged by the recovered χ^2. Results are expressed as mean values $\pm$ standard deviation.

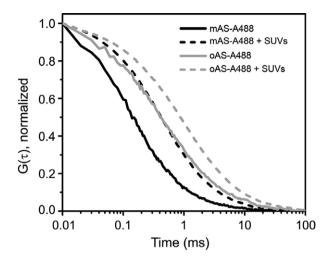# Results

Quantification of AS–membrane interaction by FCS

FCS has been widely used to study interactions between biomolecules both *in vitro* as in living cells (Schwille 2001; Jameson *et al.* 2009) and has proven valuable to quantify protein binding to biomembranes, including mAS (Rusu *et al.* 2004; Rhoades *et al.* 2006; Middleton and Rhoades 2010). We used this powerful technique to determine the impact of oligomerization on AS binding to lipid vesicles.

Diffusion of individual fluorescent particles in and out of a small observation volume gives rise to intensity fluctuations in the emitted light. The analysis of such fluctuations provides autocorrelation curves that contain information about the characteristic diffusion time of the particles (eqn 2). In a binding experiment where only one of the interacting particles is fluorescent, complex formation will be detected as an increment of the diffusion time owing to a change in the apparent molecular size of the fluorescent particle. In our case, the distinguishable species will be two, namely the labeled protein free in solution and bound to the vesicles. The experiments were performed using mAS labeled at position 140 with Alexa488 (mAS-A488). This position was chosen to prevent any interference of the hydrophobic dye on protein binding since the interaction is mediated by the N-terminal and central regions both in the monomeric (Davidson *et al.* 1998; Eliezer *et al.* 2001; Bodner *et al.* 2009; Fusco *et al.* 2014) and oligomeric (van Rooijen *et al.* 2009b; Fusco *et al.* 2017) states. Labeled oligomers (oAS-A488) were prepared from appropriate mixtures of non-labeled and labeled monomeric proteins as described in the experimental section.

Figure 2 shows representative autocorrelation curves of mAS-A488 and oAS-A488 in the absence and in the presence of an excess amount of SUVs composed of POPG. The characteristic diffusion time of mAS-A488 was ~150 μs, whereas that for oAS-A488 was ~570 μs, consistent with the higher size of the oligomeric species as compared with the monomeric protein. In the presence of lipids, both curves shifted to higher decay times denoting a decrease in diffusion as the protein binds to the liposomes. In a titration experiment of the protein upon addition of increasing lipid concentrations, saturation is evidenced by the superposition of the autocorrelation curves. The differences in the residence time between free and bound conditions allow calculation of F_{AS}^b at different lipid concentrations according to eqn 1 from which binding curves can be built. Finally, the thermodynamic partition parameters K_p and ΔG_p^0 are obtained after fitting the binding curves with eqn 3, or alternatively the dissociation constant K_d^{app} using eqn 4. It is worth to note that the terms binding and interaction should be interpreted as partitioning of the protein between water and lipid phases and that the derived thermodynamic parameters correspond to the coupling of folding and partition equilibria and account for both hydrophobic and electrostatic interactions (White *et al.* 1998).

Fig. 2 Interaction of AS to vesicles measured by fluorescence correlation spectroscopy (FCS). Representative normalized autocorrelation curves of mAS-A488 and oAS-A488 in solution (▬) and bound to POPG SUVs (▬ ▬).

We used lipid model systems to evaluate the binding parameters of mAS-A488 and oAS-A488 to vesicles under physiological conditions. Although these artificial membranes do not reflect the complexity of cellular membranes, they allow a fine tuning of membrane physical parameters such as composition and curvature. In order to analyze curvature sensitivity we used sonicated or extruded (through a membrane with 100 nm pore size) liposomes to obtain small or large unilamellar vesicles, respectively. The diameter of such vesicles was determined by DLS, ranging from 16 to 35 nm for SUVs and from ~74 to 84 nm for LUVs, depending on the composition. This change in vesicle size represents a variation by a factor of ~3 in the mean curvature ($1/r$) of the bilayer. The mean size of SUVs resembles that of ~40 nm synaptic vesicles (Takamori *et al.* 2006). To mimic the composition and fluidity of cellular membranes, we choose phosphatidylcholine (PC) for being the most abundant zwitterionic headgroup *in vivo*, and palmitoyl-oleoyl (PO) tails to approximate the asymmetry and monounsaturations of hydrocarbon chains of natural lipids (van Meer *et al.* 2008). Since binding of AS to membranes is enhanced by negatively charged lipids, we used POPS since it is the major anionic lipid in eukaryotic cell membranes (van Meer *et al.* 2008). For the sake of comparison with previous studies, we also used the acidic POPG membrane. Considering that biological membranes do not contain high proportions of anionic lipids (van Meer *et al.* 2008), we modulated the charge density at the lipid interface by preparing a binary mixture of POPC: POPS at 70 : 30 mole ratio. Additionally, to approximate the composition and anionic content (~15%) of SVs (Takamori *et al.* 2006), we used the quaternary mixture

POPC:POPS:POPE:Chol at 40:10:25:25 mole ratio (denoted as SV-m). Finally, we used a recent protocol to isolate SVs from mouse brains (Ahmed *et al.* 2013). The ~35 nm vesicles isolated with this protocol were recognized by the anti-synaptophysin antibody, a transmembrane glycoprotein present in almost all neurons that participates in synaptic transmission.

Interaction of mAS with biomembranes

The binding of mAS to lipids has been extensively investigated due to its link to synaptic homeostasis [reviewed in (Pfefferkorn *et al.* 2012; Lashuel *et al.* 2013; Auluck *et al.* 2010)]. However, an unambiguous comparison with already published thermodynamic parameters is not straightforward due to differences in experimental conditions. For that reason, we first assessed the interaction of mAS with vesicles of different sizes and compositions under physiological conditions. For such a purpose a 100 nM protein solution in HEPES buffer (150 mM NaCl, 10 mM HEPES, pH 7.5), was titrated with increasing amounts of lipids in a range of $[L]_{acc}$ = 0-400 μM (Figure S2). The autocorrelation curves became unreliable at higher lipid concentrations probably due to scattering effects (Zustiak *et al.* 2012). It is important to note that under the timescales and conditions used in our experiments, there were no evidences of protein aggregation or vesicle tubulation/aggregation (Figure S3).

Bound mAS-A488 to SUVs formed by pure POPG, POPS and POPC at saturating conditions displayed diffusion times of τ_{AS}^{b} ~ 400-600 μs. Binding curves had hyperbolic shapes consistent with a non-cooperative interaction. As expected, titration curves indicated a higher affinity of mAS-A488 for negatively charge vesicles than for neutral membranes (Fig. 3) with partition constants K_p ~2×10^{8} for POPG, POPS and ~2×10^{6} for POPC (Fig. 4 and Table 1). In correlation with these results, a decrease in the content of anionic lipids up to 30% in the binary mixture POPC:POPS drastically diminished membrane affinity, reducing K_p ~ 100 times as compared with pure POPS (Fig. 4 and Table 1). In the case of SV-m (10% of charged lipid), the affinity was even lower with a K_p value of ~7×10^{5} (Fig. 4 and Table 1).

Similarly, we evaluated the interaction of mAS-A488 with LUVs (Figure S2). In this case, the τ_{AS}^{b} values were between 1.22 and 2.05 ms. As for SUVs, the trend in affinity followed the order POPG~POPS>POPC (K_p~ 3×10^{7}, 1.5×10^{7} and 9×10^{5}, respectively) and decreased ~100 times in the mixture POPC:POPS as compared with pure POPS (Fig. 4 and Table 1). Surprisingly, although the autocorrelation curves for mAS-A488 in the presence of large SV-m indicated some degree of interaction (Figure S2), we were not able to estimate K_p since saturation was not defined within the experimentally accessible lipid concentration range.
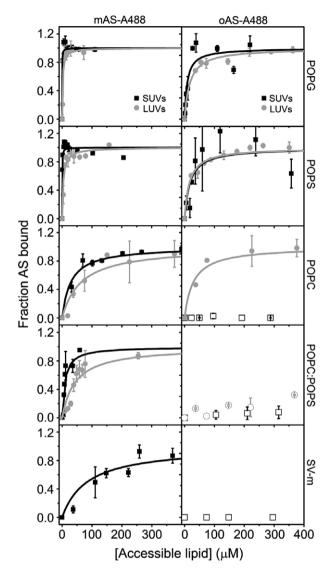
Fig. 3 Partition of distinct AS ensembles to lipid vesicles. Titration curves of mAS-A488 and oAS-A488 with SUVs (■) and LUVs (●) of different compositions derived from fluorescence correlation spectroscopy (FCS) measurements analyzed according to eqn 1. Data were fitted (■) with eqn 3 to obtain partition parameters. Open symbols (□, ○) correspond to F_{AS}^b values assuming a theoretical value for τ_{AS}^b (see text for details) and are shown only for graphical comparison. Each point corresponds to the average ± SD of at least two independent experiments.
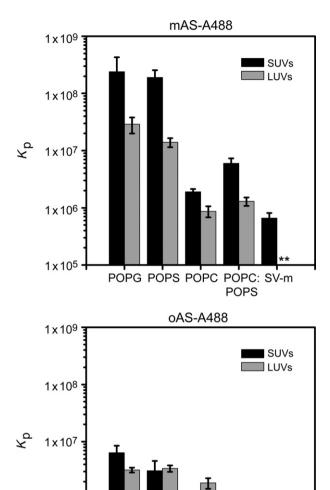

Fig. 4 Quantitative determination of the interaction of distinct AS ensembles with lipid vesicles. Partition constants of mAS-A488 and oAS-A488 to SUVs (■) and LUVs (�■) of different composition. It was not possible to estimate K_p(*) or τ_{AS}^b (**) values in some cases (see text for details). Each value corresponds to the average ± SD of at least two independent experiments.

electrostatic contribution, affect the association of AS to membranes.

Overall, our results obtained under physiological conditions are in agreement with previous reports and denote that binding of mAS is favored by anionic lipids independently of curvature membrane (Rhoades *et al.* 2006; Middleton and Rhoades 2010), without exhibiting specificity toward the headgroups of POPS or POPG (Middleton and Rhoades 2010). Furthermore, the significant values of ~−8 kcal/mol determined for POPC vesicles (Table 1) indicate that other factors, in addition to the

Regarding the influence of membrane curvature on protein binding, K_p values of mAS-A488 for SUVs were higher than those calculated for LUVs (Fig. 4 and Table 1) in agreement with a number of previous studies reporting on the higher affinity of AS for highly curved membranes (Davidson *et al.* 1998; Jo *et al.* 2000; Nuscher *et al.* 2004; Ulmer *et al.* 2005; Kamp and Beyer 2006; Kjaer *et al.* 2009; Middleton and Rhoades 2010). This sensitivity depended on vesicle composition since it decreased ~3 times in the POPC:POPS

Table 1 Apparent dissociation constant (K_d^{app}), molar coefficient partition (K_p) and free energy of partition (ΔG_p^o) for mAS-A488 and oAS-488 with vesicles varying in composition and curvature

Lipid	mAS					
	SUVs			LUVs		
	K_d^{app} (µM)	K_p	ΔG_p^o (kcal/mol)	K_d^{app} (µM)	K_p	ΔG_p^o (kcal/mol)
POPG	0.2 ± 0.1	$(2 \pm 2) \times 10^8$	−1.4 ± 0.5	1.9 ± 06	$(2.9 \pm 0.9) \times 10^7$	−10.1 ± 0.2
POPS	0.3 ± 0.1	$(1.9 \pm 0.6) \times 10^8$	−11.2 ± 0.2	4.0 ± 0.7	$(1.4 \pm 0.2) \times 10^7$	−9.7 ± 0.1
POPC	28 ± 3	$(1.9 \pm 0.2) \times 10^6$	−8.5 ± 0.1	63 ± 14	$(9 \pm 2) \times 10^5$	−8.1 ± 0.1
POPC:POPS	9 ± 2	$(6 \pm 1) \times 10^6$	−9.2 ± 0.1	44 ± 8	$(1.3 \pm 0.2) \times 10^6$	−8.3 ± 0.1
SV-m	84 ± 19	$(7 \pm 1) \times 10^5$	−7.8 ± 0.2	**	**	**

Lipid	oAS					
	SUVs			LUVs		
	K_d^{app} (µM)	K_p	ΔG_p^o (kcal/mol)	K_d^{app} (µM)	K_p	ΔG_p^o (kcal/mol)
POPG	9 ± 3	$(6 \pm 2) \times 10^6$	−9.2 ± 0.2	17 ± 2	$(3.2 \pm 0.3) \times 10^6$	−8.8 ± 0.1
POPS	18 ± 8	$(3 \pm 1) \times 10^6$	−9.0 ± 0.4	16 ± 2	$(3.4 \pm 0.4) \times 10^6$	−8.9 ± 0.1
POPC	*	*	*	29 ± 6	$(1.9 \pm 0.4) \times 10^6$	−8.5 ± 0.1
POPC:POPS	*	*	*	*	*	*
SV-m	*	*	*	**	**	**

*Undetermined.

**Undetermined τ_{AS}^b value.

mixture and ~7 times in POPC vesicles as compared to POPS vesicles (Table 1). These results suggest that under these conditions, a reduction of the electrostatic contribution to protein-membrane energetics moderates curvature dependence, as opposed to previous observations (Pranke *et al.* 2011; Chong *et al.* 2014). As expected, binding affinity of mAS-A488 for SUVs mimicking the composition of synaptic vesicles was higher than that determined for vesicles of lower curvature.

Although a number of reports point to AS as a presynaptic protein associated with SVs, to the best of our knowledge there is no published quantitative data on such interaction. Surprisingly, addition of SVs to a mAS-A488 solution did not induce any change in the autocorrelation curves (Figure S4) suggesting that K_d^{app} values are probably in the mM range. This result is in line with studies on AS subcellular localization that suggest a loose association of the protein to the distal pool of synaptic vesicles (Kahle *et al.* 2000; Fortin *et al.* 2004).

Interaction of oAS with biomembranes

We prepared sub-stoichiometrically labeled oAS-A488 that recapitulate the morphology, polydispersity, tinctorial properties, and secondary structure signatures of amyloid oligomers formed by the wild-type protein as previously reported (Celej *et al.* 2012; Gallea and Celej 2014; Gallea *et al.* 2016) (Figure S1). In parallel experiments, we

evaluated the interaction of oAS-A488 with vesicles of the same compositions and sizes as those employed for mAS-A488. Using the same population of vesicles in both cases avoids introducing differences originated from slight heterogeneities between different preparations. As before, titration experiments were performed at a fixed concentration of oligomers (1000 nM in monomeric units, ~140 nM of initial labeled protein).

With the addition of SUVs or LUVs of POPG or POPS, the autocorrelation curves shifted to higher characteristic times (τ_{AS}^u~0.8–2.9 ms) denoting binding of oligomers to the acidic membranes. The K_p values were ~3×10^6 (Fig. 4 and Table 1) in both cases, indicating that oAS-A488 do not also show specificity for the polar group of these lipids, and, more striking, that they bind with similar strengths to vesicles of both sizes. Binding affinity drastically diminished when the content of the negatively charged lipid was reduced in the mixtures POPC:POPS or SV-m (Fig. 4 and Table 1). Only a weak interaction with SV-m of low curvature was observed, although the K_p value could not be determined since saturation was not defined (Figure S2). Recently, Fusco *et al.* (2017) used FCS to qualitatively probe the interaction of AS oligomers with vesicles that mimic the composition and curvature of SVs. They observed a strong binding of oAS to SUVs composed of DOPE:DOPS:DOPC at 50:30:20 mole ratio. This lipid mixture has a higher proportion of anionic lipid, increased unsaturation chain content and lacks

cholesterol as compared to SV-m, which might explain the distinct membrane interactions observed. On the other hand, the addition of SUVs of POPC did not induce any shift in the autocorrelation curve (Figure S2) whereas a K_p value of ~2 × 10^6 was determined for LUVs (Fig. 4 and Table 1), in clear contrast to the previous observations for mAS-A488.

These results demonstrate that oligomerization has a deep impact on AS binding properties to membranes, abolishing interaction in some cases or drastically changing curvature sensitivity in others. In this regard, oligomers are no longer curvature sensors in membranes composed of pure anionic lipids but have higher affinity for zwitterionic membranes of low curvature.

We observed that τ_{AS}^b values for oAS-A488 in the presence of an excess of POPG and POPS LUVs were smaller than those determined for mAS-A488 under the same conditions (Figure S2). One plausible explanation for this unexpected result would be the presence of a fraction of oligomers that contribute to the observed signal but that do not participate in the partition equilibrium leading to smaller correlation times. It has been reported that membrane-induced AS aggregation involves lipid extraction from the bilayer and the clustering of membrane around protein aggregates (Reynolds et al. 2011; Hellstrand et al. 2013; Chaudhary et al. 2014). Aggregates formed on supported bilayers were recognized by the anti-oligomer antibody A11, and it was suggested that addition of pre-formed oligomers to membranes could result in the extraction of a small amount of lipids (Reynolds et al. 2011). Moreover, oAS prepared by the lyophilization method are able to induce leakage from POPG or POPS liposomes (van Rooijen et al. 2009a; Gallea et al. 2016; Fusco et al. 2017). It was shown that membrane permeabilization is due to non-equilibrium processes causing a rapid dye efflux due to bilayer defects arising from intrinsic membrane instability, but that the overall vesicle morphology remains unaltered (van Rooijen et al. 2010). Thus, it might be possible that oligomers containing lipids would be formed during the equilibration time, which are then unable to interact with the vesicle, remaining as free diffusing particles in solution during the measurement.

As for the monomeric protein, the autocorrelation curves for oAS-A488 did not shift with the addition of SVs (Figure S4) also suggesting a low affinity for this natural membrane.

Discussion

The interaction of AS with membranes has attracted much attention since it might play a key role in the pathophysiology linked to this protein. Although the exact function of AS remains elusive, there is a general consensus on its participation in the maintenance of the reserve pool of synaptic vesicles and in the regulation of vesicle fusion and dynamics (Auluck et al. 2010; Lashuel et al. 2013).

Monomeric AS is a curvature sensor protein exhibiting an exquisite sensitivity toward anionic vesicles similar in size to SVs (Antonny 2011; Pranke et al. 2011), supporting its physiological role in synaptic homeostasis. On the other hand, cellular damage is one of the cytotoxic mechanisms attributed to oligomeric species of AS which are considered the most neurotoxic species (Lashuel et al. 2013; Chiti and Dobson 2017). However, oligomers might be also toxic to neurons by a loss-of-function mechanism not only due to a decrease of protein available to exert its function but also due to altered membrane binding properties. In this regard, in this work we aimed at deciphering the impact of oligomerization on AS curvature membrane sensitivity.

We determined that under physiological conditions mAs bind to SUVs and LUVs of POPG or POPS with similar affinities (Fig. 3 and Table 1) indicating no particular specificity for these polar head groups in agreement with previous results (Zhu et al. 2003; Middleton and Rhoades 2010). We also determined that the interaction is favored by the increase in the negative charge density of the lipid interface and curvature bilayer as previously reported (Davidson et al. 1998; Rhoades et al. 2006; Middleton and Rhoades 2010; Pranke et al. 2011). As mentioned before, AS interacts with synaptic-like vesicles through its N-terminal anchor which enhances the binding of the membrane-sensor central region to the lipid surface (Fusco et al. 2014). The dual sensitivity to both charge and curvature has been explained in terms of the particular chemical characteristics of the extended amphipathic helix formed at the N-terminal and central protein domains (residues ~Met^1-Ala^{90}) (Jao et al. 2008) upon binding to lipid vesicles (Antonny 2011; Pranke et al. 2011). In contrast to classic amphipathic helices, α-synuclein bears a poor hydrophobic phase and a well-developed charged polar face with an almost even distribution of positively charged residues at its two edges (Antonny 2011; Pranke et al. 2011) (Fig. 1b). Pranke et al. (2011) suggested that membrane curvature would facilitate the insertion of the amphipathic helix in the interfacial region and that the minimal contribution of the hydrophobic face is overcome by electrostatic interactions. However, the calculated values (Table 1) which include both hydrophobic and electrostatic interactions, indicate that the former should not be underestimated. Assuming that the hydrophobic contribution is similar in vesicles formed by POPG, POPS, POPC, and POPC:POPS, the values suggest that the insertion of hydrophobic residues and the hydrocarbon side chains of Lys (Mishra et al. 1994) into the bilayer significantly contribute to membrane-protein interaction. Strikingly, this contribution is higher for highly curved vesicles as judged by the values determined for SUVs and LUVs of POPC (Table 1). On the basis of these results we suggest that the hydrophobic contribution is the thermodynamic driving force underlying the association of AS with membranes, possibly to compensate for lipid packing defects that are especially

prominent in small vesicles (Nuscher *et al.* 2004; Antonny 2011).

There are contradictory results regarding the binding of AS to zwitterionic membranes. Whereas some authors reported that AS is unable to bind to membranes of POPC (Davidson *et al.* 1998) or to a mixture of PC:POPE:Cholesterol (except a weak interaction with highly curved liposomes) (Pranke *et al.* 2011), others have reported different affinities for POPC vesicles (this work and (Rhoades *et al.* 2006; Middleton and Rhoades 2010; Iyer *et al.* 2016; Narayanan and Scarlata 2001; Jiang *et al.* 2013). These discrepancies could arise from differences in experimental conditions, liposome sizes, or compositions. A recent study demonstrated that the addition of cholesterol to POPC membranes completely abolishes AS binding (Iyer *et al.* 2016) which could be explained by the lipid ordering induced by cholesterol and the reduced affinity of AS for the liquid-order phase (Stöckl *et al.* 2008; Galvagnion *et al.* 2016). These findings could conceal the behavior observed in the PC:POPE:Cholesterol mixture (Pranke *et al.* 2011). It is interesting to note that AS is able to bind vesicles containing 25% of cholesterol and only 10% of anionic lipids in the lipid mixture that mimic the composition and curvature of synaptic vesicles (Fig. 3 and Table 1) consistent with the proposed physiological function of AS (Auluck *et al.* 2010; Lashuel *et al.* 2013).

Different aggregated states are able to associate with lipid membranes (Volles *et al.* 2001; Giannakis *et al.* 2008; van Rooijen *et al.* 2009a; Pfefferkorn *et al.* 2012). oAS ensembles produced with experimental protocols similar to that used in the present work, share some of the binding properties displayed by mAS, such as a greater selectivity for anionic membranes in liquid-disordered phase (van Rooijen *et al.* 2008). In addition, oAS-lipid interaction is also mediated by the N-terminal and central domains of the protein, at least up to residue Ala[90] (van Rooijen *et al.* 2009b; Fusco *et al.* 2017). Here we quantitatively show that neither mAS nor oAS have the capacity to distinguish between PG and PS head groups, since they bind to both lipids with similar strength (Figure 4 and Table 1; see also ref. [Middleton and Rhoades 2010]).

However, our results demonstrate that oligomerization deeply affects the interaction of AS with membranes (Figs 3 and 4, and Table 1). Binding affinity diminishes and the interaction is completely abolished in some cases. Importantly, in the lipid mixture that mimic the composition of synaptic vesicles, oAS do not bind to highly curved vesicles and interact poorly with those of low curvature (Fig. 3). In addition, oligomers are insensitive to curvature in membranes composed of pure anionic lipids and bind to LUVs made purely with the zwitterionic lipid POPC.

These drastic changes regarding curvature sensitivity could arise from conformational restrictions imposed to the protein in the oligomeric aggregate. As mentioned before, the N-terminal and central regions of the protein participate in lipid interactions both in the monomeric and oligomeric state (van Rooijen

et al. 2009b; Fusco *et al.* 2017). If these regions would be hidden or conformationally constrained within the interior of the oligomeric state, the anchoring and membrane-sensitivity properties (Pranke *et al.* 2011; Fusco *et al.* 2014) will be largely affected. Circular dichroism studies indicate that oAS do not undergo significant conformational changes upon binding to membranes (Volles and Lansbury 2002; van Rooijen *et al.* 2009a), which could suggest the lack of structuring of the N-terminal and central regions into the distinct extended amphipathic helix. Within the oligomeric core spanning residues Phe[4]–Ala[90] (van Rooijen *et al.* 2009b), discrete segments Phe[4]–Ala[17], Tyr[39]–Thr[54], and Val[70]–Ala[89] exhibit stable hydrogen-bonded or solvent-shielded structures (Mysling *et al.* 2013) and a tight packing with a distinct pattern of intermolecular contacts at least for the region encompassing residues Ser[9]–Ala[76] likely reflecting the adoption of a well-defined structure (Gallea and Celej 2014). More recently, C^{13}-C^{13} dipolar assisted rotational resonance measurements showed that the first ~N-terminal 25 residues of oligomers produced using a similar protocol, adopt an helical conformation upon interacting with lipid assemblies that mimic synaptic-like lipid membranes (Fusco *et al.* 2017). Bioinformatic analysis using the COILS algorithm predicts a modest coiled-coil propensity (~2%) for the first 21 residues of the protein. If these residues were engaged in such conformation, the hydrophobic residues would be sequestered from the solvent by facing each other, whereas the charged residues, especially Lys, would be exposed. In this scenario, basic patches on the surface of oAS would mediate the interaction with anionic lipids but would be insensitive to curvature changes. On the other hand, oAS exhibit solvent-exposed hydrophobic patches (Chen *et al.* 2015; Gallea *et al.* 2016), which could mediate the association to zwitterionic membranes of low curvature or even flat interfaces (Quist *et al.* 2005; Kim *et al.* 2009). It is well known that oligomer binding to biological membranes, such as the mitochondrial or plasma membranes, would compromise cell viability by impairing lipid membrane integrity. In this connection, it has been recently shown that oligomers produced by the lyophilization method that bind and disrupt cellular membranes leading to neural toxicity, have an exposed lipophilic region and a core rich in antiparallel β-sheet structure (Fusco *et al.* 2017), both structural elements featured by our oligomeric preparation.

In healthy neurons, transient interactions of AS with synaptic vesicles could assist in vesicle stabilization, possibly by releasing curvature stress, thereby protecting them from premature fusion and holding them in a reserve pool distal from the synapse (Auluck *et al.* 2010). Under pathological conditions, a decrease in the amount of functional AS would cause a depletion of this reservoir, as these vesicles would either degrade or fuse very efficiently with their target membranes (Auluck *et al.* 2010). This work presents quantitative evidences pointing toward a loss-of-function mechanism of oAS toxicity, not only by decreasing the availability

of functional protein but also by the incapacity of the oligomeric species of recognizing or remaining bound to synaptic vesicles. This novel mechanism would contribute to cellular dysfunction along with the well-established pathological pathway associated to the impairment of membrane integrity, pore formation, and cellular homeostasis.

Acknowledgments and conflict of interest disclosure

Open Science Badges

This article has received a badge for *Open Materials* because it provided all relevant information to reproduce the study in the manuscript. The complete Open Science Disclosure form for this article can be found at the end of the article. More information about the Open Practices badges can be found at https://cos.io/our-services/open-science-badges/.

Supporting information

Additional supporting information may be found online in the Supporting Information section at the end of the article.

Figure S1. General properties of oAS-A488 compared with mAS-A488.

Figure S2. Normalized autocorrelation curves of mAS-A488 and oAS-A488 at increasing accessible lipid concentrations for different vesicle compositions.

Figure S3. Protein and vesicle stability under FCS conditions.

Figure S4. Synuclein interaction with synaptic vesicles.

References

Ahmed S., Holt M., Riedel D. and Jahn R. (2013) Small-scale isolation of synaptic vesicles from mammalian brain. *Nat. Protoc.* **8**, 998–1009.

Antonny B. (2011) Mechanisms of membrane curvature sensing. *Annu. Rev. Biochem.* **80**, 101–123.

Auluck P. K., Caraveo G. and Lindquist S. (2010) α-Synuclein: membrane interactions and toxicity in Parkinson's disease. *Annu. Rev. Cell Dev. Biol.* **26**, 211–233.

Bodner C. R., Dobson C. M. and Bax A. (2009) Multiple tight phospholipid-binding modes of alpha-synuclein revealed by solution NMR spectroscopy. *J. Mol. Biol.* **390**, 775–790.

Burré J., Sharma M., Tsetsenis T., Buchman V., Etherton M. R. and Südhof T. C. (2010) Alpha-synuclein promotes SNARE-complex assembly in vivo and in vitro. *Science* **329**, 1663–1667.

Cabin D. E., Shimazu K., Murphy D. *et al.* (2002) Synaptic vesicle depletion correlates with attenuated synaptic responses to prolonged repetitive stimulation in mice lacking alpha-synuclein. *J. Neurosci.* **22**, 8797–8807.

Celej M. S., Sarroukh R., Goormaghtigh E., Fidelio G. D., Ruysschaert J. M. and Raussens V. (2012) Toxic prefibrillar α-synuclein amyloid oligomers adopt a distinctive antiparallel β-sheet structure. *Biochem. J.* **443**, 719–726.

Chandra S., Gallardo G., Fernández-Chacón R., Schlüter O. M. and Südhof T. C. (2005) Alpha-synuclein cooperates with CSPalpha in preventing neurodegeneration. *Cell* **123**, 383–396.

Chaudhary H., Stefanovic A. N., Subramaniam V. and Claessens M. M. (2014) Membrane interactions and fibrillization of α-synuclein play an essential role in membrane disruption. *FEBS Lett.* **588**, 4457–4463.

Chen S. W., Drakulic S., Deas E. *et al.* (2015) Structural characterization of toxic oligomers that are kinetically trapped during α-synuclein fibril formation. *Proc. Natl Acad. Sci. USA* **112**, E1994–E2003.

Chiti F. and Dobson C. M. (2017) Protein misfolding, amyloid formation, and human disease: a summary of progress over the last decade. *Annu. Rev. Biochem.* **86**, 27–68.

Chong S. S., Taneva S. G., Lee J. M. and Cornell R. B. (2014) The curvature sensitivity of a membrane-binding amphipathic helix can be modulated by the charge on a flanking region. *Biochemistry* **53**, 450–461.

Cremades N., Chen S. W. and Dobson C. M. (2017) Structural characteristics of α-synuclein oligomers. *Int Rev Cell Mol Biol* **329**, 79–143.

Davidson W. S., Jonas A., Clayton D. F. and George J. M. (1998) Stabilization of a-synuclein secondary structure upon binding to synthetic membranes. *J. Biol. Chem.* **273**, 9443–9449.

Diao J., Burré J., Vivona S., Cipriano D. J., Sharma M., Kyoung M., Südhof T. C. and Brunger A. T. (2013) Native α-synuclein induces clustering of synaptic-vesicle mimics via binding to phospholipids and synaptobrevin-2/VAMP2. *Elife* **2**, e00592.

Dickey A. and Faller R. (2008) Examining the contributions of lipid shape and headgroup charge on bilayer behavior. *Biophys. J.* **95**, 2636–2646.

Eliezer D., Kutluay E., Bussell R., Jr and Browne G. (2001) Conformational properties of alpha-synuclein in its free and lipid-associated states. *J. Mol. Biol.* **307**, 1061–1073.

Fiske C. H. (1925) The colorimetric determination of phosphorus. in *J. Biol. Chem.*, (Y. Subbarow ed.), **66**, pp. 375–400.

Fortin D. L., Troyer M. D., Nakamura K., Kubo S., Anthony M. D. and Edwards R. H. (2004) Lipid rafts mediate the synaptic localization of alpha-synuclein. *J. Neurosci.* **24**, 6715–6723.

Fusco G., De Simone A., Gopinath T., Vostrikov V., Vendruscolo M., Dobson C. M. and Veglia G. (2014) Direct observation of the three regions in α-synuclein that determine its membrane-bound behaviour. *Nat. Commun.* **5**, 3827.

Fusco G., Chen S. W., Williamson P. T. F. *et al.* (2017) Structural basis of membrane disruption and cellular toxicity by α-synuclein oligomers. *Science* **358**, 1440–1443.

Gallea J. I. and Celej M. S. (2014) Structural insights into amyloid oligomers of the Parkinson disease-related protein α-synuclein. *J. Biol. Chem.* **289**, 26733–26742.

Gallea J. I., Sarroukh R., Yunes-Quartino P., Ruysschaert J. M., Raussens V. and Celej M. S. (2016) Structural remodeling during amyloidogenesis of physiological Nα-acetylated α-synuclein. *Biochim. Biophys. Acta* **1864**, 501–510.

Galvagnion C., Brown J. W., Ouberai M. M., Flagmeier P., Vendruscolo M., Buell A. K., Sparr E. and Dobson C. M. (2016) Chemical

properties of lipids strongly affect the kinetics of the membrane-induced aggregation of α-synuclein. *Proc. Natl Acad. Sci. USA* **113**, 7065–7070.

Giannakis E., Pacífico J., Smith D. P., Hung L. W., Masters C. L., Cappai R., Wade J. D. and Barnham K. J. (2008) Dimeric structures of alpha-synuclein bind preferentially to lipid membranes. *Biochim. Biophys. Acta* **1778**, 1112–1119.

Haugland R. P. and Spence M. T. Z. (2005) The handbook : a guide to fluorescent probes and labeling technologies. Invitrogen, [United States].

Hellstrand E., Nowacka A., Topgaard D., Linse S. and Sparr E. (2013) Membrane lipid co-aggregation with α-synuclein fibrils. *PLoS ONE* **8**, e77235.

Ingelsson M. (2016) Alpha-synuclein oligomers-neurotoxic molecules in Parkinson's disease and other lewy body disorders. *Front Neurosci.* **10**, 408.

Iwai A., Masliah E., Yoshimoto M., Ge N., Flanagan L., de Silva H. A., Kittel A. and Saitoh T. (1995) The precursor protein of non-A beta component of Alzheimer's disease amyloid is a presynaptic protein of the central nervous system. *Neuron* **14**, 467–475.

Iyer A., Roeters S. J., Schilderink N., Hommersom B., Heeren R. M., Woutersen S., Claessens M. M. and Subramaniam V. (2016) The Impact of N-terminal Acetylation of α-Synuclein on Phospholipid Membrane Binding and Fibril Structure. *J. Biol. Chem.* **291**, 21110–21122.

Jameson D. M., Ross J. A. and Albanesi J. P. (2009) Fluorescence fluctuation spectroscopy: ushering in a new age of enlightenment for cellular dynamics. *Biophys Rev.* **1**, 105–118.

Jao C. C., Hegde B. G., Chen J., Haworth I. S. and Langen R. (2008) Structure of membrane-bound alpha-synuclein from site-directed spin labeling and computational refinement. *Proc. Natl Acad. Sci. USA* **105**, 19666–19671.

Jiang Z., de Messieres M. and Lee J. C. (2013) Membrane remodeling by alpha-synuclein and effects on amyloid formation. *J. Am. Chem. Soc.* **135**, 15970–15973.

Jo E., McLaurin J., Yip C. M., St George-Hyslop P. and Fraser P. E. (2000) alpha-Synuclein membrane interactions and lipid specificity. *J. Biol. Chem.* **275**, 34328–34334.

Kahle P. J., Neumann M., Ozmen L. *et al.* (2000) Subcellular localization of wild-type and Parkinson's disease-associated mutant alpha -synuclein in human and transgenic mouse brain. *J. Neurosci.* **20**, 6365–6373.

Kamp F. and Beyer K. (2006) Binding of alpha-synuclein affects the lipid packing in bilayers of small vesicles. *J. Biol. Chem.* **281**, 9251–9259.

Kim H. Y., Cho M. K., Kumar A. *et al.* (2009) Structural properties of pore-forming oligomers of alpha-synuclein. *J. Am. Chem. Soc.* **131**, 17482–17489.

Kjaer L., Giehm L., Heimburg T. and Otzen D. (2009) The influence of vesicle size and composition on alpha-synuclein structure and stability. *Biophys. J .* **96**, 2857–2870.

Larsen K. E., Schmitz Y., Troyer M. D. *et al.* (2006) Alpha-synuclein overexpression in PC12 and chromaffin cells impairs catecholamine release by interfering with a late step in exocytosis. *J. Neurosci.* **26**, 11915–11922.

Lashuel H. A., Overk C. R., Oueslati A. and Masliah E. (2013) The many faces of α-synuclein: from structure and toxicity to therapeutic target. *Nat. Rev. Neurosci.* **14**, 38–48.

Masuda M., Dohmae N., Nonaka T., Oikawa T., Hisanaga S., Goedert M. and Hasegawa M. (2006) Cysteine misincorporation in bacterially expressed human alpha-synuclein. *FEBS Lett.* **580**, 1775–1779.

van Meer G., Voelker D. R. and Feigenson G. W. (2008) Membrane lipids: where they are and how they behave. *Nat. Rev. Mol. Cell Biol.* **9**, 112–124.

Middleton E. R. and Rhoades E. (2010) Effects of curvature and composition on α-synuclein binding to lipid vesicles. *Biophys. J .* **99**, 2279–2288.

Mishra V. K., Palgunachari M. N., Segrest J. P. and Anantharamaiah G. M. (1994) Interactions of synthetic peptide analogs of the class A amphipathic helix with lipids. Evidence for the snorkel hypothesis. *J. Biol. Chem.* **269**, 7185–7191.

Murphy D. D., Rueter S. M., Trojanowski J. Q. and Lee V. M. (2000) Synucleins are developmentally expressed, and alpha-synuclein regulates the size of the presynaptic vesicular pool in primary hippocampal neurons. *J. Neurosci.* **20**, 3214–3220.

Mysling S., Betzer C., Jensen P. H. and Jorgensen T. J. (2013) Characterizing the dynamics of alpha-synuclein oligomers using hydrogen/deuterium exchange monitored by mass spectrometry. *Biochemistry* **52**, 9097–9103.

Narayanan V. and Scarlata S. (2001) Membrane binding and self-association of alpha-synucleins. *Biochemistry* **40**, 9927–9934.

Nemani V. M., Lu W., Berge V., Nakamura K., Onoa B., Lee M. K., Chaudhry F. A., Nicoll R. A. and Edwards R. H. (2010) Increased expression of alpha-synuclein reduces neurotransmitter release by inhibiting synaptic vesicle reclustering after endocytosis. *Neuron* **65**, 66–79.

Nuscher B., Kamp F., Mehnert T., Odoy S., Haass C., Kahle P. J. and Beyer K. (2004) Alpha-synuclein has a high affinity for packing defects in a bilayer membrane: a thermodynamics study. *J. Biol. Chem.* **279**, 21966–21975.

Pfefferkorn C. M., Jiang Z. and Lee J. C. (2012) Biophysics of alpha-synuclein membrane interactions. *Biochim. Biophys. Acta* **1818**, 162–171.

Pranke I. M., Morello V., Bigay J., Gibson K., Verbavatz J. M., Antonny B. and Jackson C. L. (2011) α-Synuclein and ALPS motifs are membrane curvature sensors whose contrasting chemistry mediates selective vesicle binding. *J. Cell Biol.* **194**, 89–103.

Quist A., Doudevski I., Lin H., Azimova R., Ng D., Frangione B., Kagan B., Ghiso J. and Lal R. (2005) Amyloid ion channels: a common structural link for protein-misfolding disease. *Proc. Natl Acad. Sci. USA* **102**, 10427–10432.

Reynolds N. P., Soragni A., Rabe M., Verdes D., Liverani E., Handschin S., Riek R. and Seeger S. (2011) Mechanism of membrane interaction and disruption by α-synuclein. *J. Am. Chem. Soc.* **133**, 19366–19375.

Rhoades E., Ramlall T. F., Webb W. W. and Eliezer D. (2006) Quantification of alpha-synuclein binding to lipid vesicles using fluorescence correlation spectroscopy. *Biophys. J .* **90**, 4692–4700.

van Rooijen B. D., Claessens M. M. and Subramaniam V. (2008) Membrane binding of oligomeric alpha-synuclein depends on bilayer charge and packing. *FEBS Lett.* **582**, 3788–3792.

van Rooijen B. D., Claessens M. M. and Subramaniam V. (2009a) Lipid bilayer disruption by oligomeric alpha-synuclein depends on bilayer charge and accessibility of the hydrophobic core. *Biochim. Biophys. Acta* **1788**, 1271–1278.

van Rooijen B. D., van Leijenhorst-Groener K. A., Claessens M. M. and Subramaniam V. (2009b) Tryptophan fluorescence reveals structural features of alpha-synuclein oligomers. *J. Mol. Biol.* **394**, 826–833.

van Rooijen B. D., Claessens M. M. and Subramaniam V. (2010) Membrane Permeabilization by Oligomeric alpha-Synuclein. In Search of the Mechanism. *PLoS ONE* **5**, e14292.

Rusu L., Gambhir A., McLaughlin S. and Rädler J. (2004) Fluorescence correlation spectroscopy studies of Peptide and protein binding to phospholipid vesicles. *Biophys. J .* **87**, 1044–1053.

Schwille P. (2001) Fluorescence correlation spectroscopy and its potential for intracellular applications. *Cell Biochem. Biophys.* **34**, 383–408.

Stöckl M., Fischer P., Wanker E. and Herrmann A. (2008) Alpha-synuclein selectively binds to anionic phospholipids embedded in liquid-disordered domains. *J. Mol. Biol.* **375**, 1394–1404.

Takamori S., Holt M., Stenius K. *et al.* (2006) Molecular anatomy of a trafficking organelle. *Cell* **127**, 831–846.

Thompson N. L. (1991) Fluorescence correlation spectroscopy. pp. 337–378. Lakowicz, J. R., Topics in Fluorescence Microscopy.

Ulmer T. S., Bax A., Cole N. B. and Nussbaum R. L. (2005) Structure and dynamics of micelle-bound human alpha-synuclein. *J. Biol. Chem.* **280**, 9595–9603.

Volles M. J. and Lansbury P. T., Jr (2002) Vesicle permeabilization by protofibrillar alpha-synuclein is sensitive to Parkinson's disease-linked mutations and occurs by a pore-like mechanism. *Biochemistry* **41**, 4595–4602.

Volles M. J., Lee S. J., Rochet J. C., Shtilerman M. D., Ding T. T., Kessler J. C. and Lansbury P. T. (2001) Vesicle permeabilization by protofibrillar alpha-synuclein: implications for the pathogenesis and treatment of Parkinson's disease. *Biochemistry* **40**, 7812–7819.

White S. H., Wimley W. C., Ladokhin A. S. and Hristova K. (1998) Protein folding in membranes: determining energetics of peptide-bilayer interactions. *Methods Enzymol.* **295**, 62–87.

Zhu M., Li J. and Fink A. L. (2003) The association of alpha-synuclein with membranes affects bilayer structure, stability, and fibril formation. *J. Biol. Chem.* **278**, 40186–40197.

Zustiak S., Riley J., Boukari H., Gandjbakhche A. and Nossal R. (2012) Effects of multiple scattering on fluorescence correlation spectroscopy measurements of particles moving within optically dense media. *J. Biomed. Opt.* **17**, 125004.

Open Practices Disclosure

Manuscript Title: Amyloid oligomerization of the Parkinson's disease related protein α-synuclein impacts on its curvature-membrane sensitivity.
Corresponding Author: Maria Soledad Celej

Articles accepted to *Journal of Neurochemistry* after 01.2018 are eligible to earn badges that recognize open scientific practices: publicly available data, material, or preregistered research plans. Please read more about the badges in our *author guidelines and Open Science Badges page*, and you can also find information on the Open Science Framework wiki.

[X] Please check this box if you are interested in participating.

To apply for one or more badges acknowledging open practices, please check the box(es) corresponding to the desired badge(s) below and provide the information requested in the relevant sections. To qualify for a badge, you must provide a URL, doi, or other permanent path for accessing the specified information in a public, open-access repository. **Qualifying public, open-access repositories are committed to preserving data, materials, and/or registered analysis plans and keeping them publicly accessible via the web in perpetuity.** Examples include the Open Science Framework (OSF) and the various Dataverse networks. Hundreds of other qualifying data/materials repositories are listed at http://re3data.org/. Preregistration of an analysis plan must take place via a publicly accessible registry system (e.g., OSF, ClinicalTrials.gov or other trial registries in the WHO Registry Network, institutional registration systems). **Personal websites and most departmental websites do not qualify as repositories.**

Authors who wish to publicly post third-party material in their data, materials, or preregistration plan must have the proper authority or permission agreement in order to do so.

There are circumstances in which it is not possible or advisable to share any or all data, materials, or a research plan publicly. For example, there are cases in which sharing participants' data could violate confidentiality. If you would like your article to include an explanation of such circumstances and/or provide links to any data or materials you have made available—even if not under conditions eligible to earn a badge—you may write an alternative note that will be published in a note in the article**.** Please check this box if you would like your article to include an alternative note and provide the text of the note below:

[] Alternative note:

[] Open Data Badge

1. Provide the URL, doi, or other **permanent path** for accessing the data in a **public, open-access repository**:

> **[]** Confirm that there is sufficient information for an independent researcher to reproduce **all of the reported results**, including codebook if relevant.

> **[]** Confirm that you have registered the uploaded files so that they are **time stamped** and cannot be age.

[X] Open Materials Badge

> 1.   Provide the URL, doi, or other **permanent path** for accessing the materials in a **public, open-access repository**: all relevant information is provided in the manuscript.

> **[X]** Confirm that there is sufficient information for an independent researcher to reproduce **all of the reported methodology**.

> **[]** Confirm that you have registered the uploaded files so that they are **time stamped** and cannot be age.

[] Preregistered Badge

> 1.   Provide the URL, doi, or other **permanent path** to the registration in a **public, open-access repository***:

2. Was the analysis plan registered prior to examination of the data or observing the outcomes? If no, explain.**

3. Were there additional registrations for the study other than the one reported? If yes, provide links and explain.*

*No badge will be awarded if (1) is not provided, **or** if (3) is answered "yes" without strong justification

**If the answer to (2) is "no," the notation DE (Data Exist) will be added to the badge, indicating that registration postdates realization of the outcomes but predates analysis.

By signing below, authors affirm that the above information is accurate and complete, that any third-party material has been reproduced or otherwise made available only with the permission of the original author or copyright holder, and that publicly posted data do not contain information that would allow individuals to be identified without consent.

Date: 2018/08/17

Name: Maria Soledad Celej

Signature: